

General theory of heat diffusion dynamics

A. Tröster* and W. Schranz

Institut für Experimentalphysik, Universität Wien, Strudlhofgasse 4, A-1090 Wien, Austria

(Received 4 July 2002; revised manuscript received 11 September 2002; published 27 November 2002)

A detailed theoretical investigation of the influence of heat diffusion processes on the low-frequency dispersion in macroscopic elastic susceptibilities is presented. In particular, a general solution of the heat diffusion equation is derived for arbitrary boundary conditions and externally imposed periodic and spatially inhomogeneous stress. In contrast to other calculations found in the literature, our results indicate that in elastic experiments on monodomain samples of macroscopic dimensions the isothermal-adiabatic crossover function necessarily reduces to a Debye-like dispersion. Experimentally, this is illustrated by measurements of the complex dynamic elastic susceptibilities of KSCN and KMnF₃. Our approach also allows to discuss heat diffusion in polydomain crystals and heterogeneous systems, for which one obtains dispersions of a non-Debye type. While explicitly derived in an elastic context, the present theory also applies to heat diffusion in dielectric materials.

DOI: 10.1103/PhysRevB.66.184110

PACS number(s): 62.20.-x, 62.40.+i, 66.70.+f

I. INTRODUCTION

Historically, the problem of ultralow-frequency dynamics near structural phase transitions is intimately related to the observation of so-called central peaks, which in the 1970s were mainly investigated using scattering methods.¹⁻³ Very recently the field was revived due to the works of Chaves *et al.*⁴⁻⁶ who investigated the influence of heat-diffusion processes on *macroscopic* susceptibilities of ferroelectric materials both theoretically and experimentally. Chaves *et al.* looked for heat-diffusion central peaks in the complex dielectric susceptibilities of a number of ferroelectric crystals. In particular, the authors predicted that the crossover from isothermal to adiabatic conditions (i.e., from low to high frequencies) is determined by a certain non-Debye-like dispersion function. Also, in the recent work of Fally *et al.*⁷ a different non-Debye isothermal-adiabatic crossover function was calculated for the dielectric susceptibility of ferroelectric materials. At the same time Schranz *et al.*^{8,9} began to study the influence of heat diffusion dynamics using *elastic* measurements. In Ref. 8 they clearly observed Debye relaxation in the low-frequency elastic susceptibility of the molecular crystal KSCN which was shown to originate from heat diffusion dynamics. Very recently⁹ signs of a Debye crossover from an isothermal to adiabatic regime have been found in KMnF₃ crystals. Our present paper addresses the question of which type of isothermal-adiabatic crossover function is to be expected in elastic measurements under realistic experimental conditions. Specifically, we present a general three-dimensional theory which describes the influence of heat propagation on the dynamic properties of macroscopic susceptibilities, addresses the crucial influence of the boundary conditions, and coherently relates the different dispersion functions found in the literature. Our results are explicitly calculated for crystals subject to external stresses $\boldsymbol{\sigma}$, however, they correspondingly apply to dielectrically induced heat diffusion in an obvious way. We therefore prefer to generally speak of $\boldsymbol{\sigma}$ as an *external excitation* in what follows below.

II. ELASTIC MEASUREMENTS

Consider a crystal of volume V subject to a static external force applied to a point or area of the crystal's surface in a way to be specified later. Within linear-response theory we assume that the crystal responds by a reacting force $\chi^T \zeta$ linear in the corresponding elongation ζ . This force is the result of a stress field $\sigma_i(\mathbf{r})$ ($i=1, \dots, 6$), produced within V , and conservation of mechanical energy demands that

$$E_m := \int_0^{\zeta_0} d\zeta \chi^T \zeta = \frac{\zeta_0^2}{2\chi^T} \equiv \frac{1}{2} \sum_{ij} S_{ij}^T \langle \sigma_i \sigma_j \rangle_{L_2}, \quad (1)$$

where $\langle \sigma_i \sigma_j \rangle_{L_2} := \int_V d^3r \sigma_i(\mathbf{r}) \sigma_j(\mathbf{r})$, and S_{ij}^T denotes the crystal's isothermal compliances. From this we conclude that statically $\chi^T f_0^2 = \sum_{ij} S_{ij}^T \langle \sigma_i \sigma_j \rangle$, where $f_0 := \chi^T \zeta_0$. In the case of a dynamic external force $f(t) = f_0 \cos[\omega t]$, suppose that the system's long-time response is

$$\zeta(t) = \hat{\zeta}_0(\omega) \cos[\omega t - \delta(\omega)]. \quad (2)$$

$0 < \delta(\omega) < \pi$ describes the loss in mechanical energy. Generalizing the above static relation, we define

$$\chi(\omega) f_0^2 \equiv \sum_{ij} S_{ij}(\omega) \langle \sigma_i \sigma_j \rangle_{L_2}, \quad (3)$$

where $\chi(\omega)$ and $S_{ij}(\omega)$ are the complex frequency-dependent mechanical susceptibility and elastic compliance. In general, measuring of $\chi(\omega)$ determines a combination of compliances $S_{ij}(\omega)$. However, if $\sigma_i(\mathbf{x}) = \delta_{ik} \sigma_k(\mathbf{x})$, then $S_{kk}(\omega)$ is determined by $\chi(\omega)$ via

$$S_{kk}(\omega) \equiv \frac{f_0^2}{\|\sigma_k\|_{L_2}^2} \chi(\omega). \quad (4)$$

The mechanical work done on the system is $E_m(t) = \int_{t_0}^t f(s) \dot{\zeta}(s) ds$. Averaged over one period, we obtain

$$\left\langle \frac{dE_m}{dt} \right\rangle = \frac{\omega}{2\pi} \int_0^{2\pi/\omega} dt \dot{E}_m(t) = \frac{f_0}{2} \hat{\zeta}_0(\omega) \omega \sin \delta(\omega). \quad (5)$$

In complex form, one defines $\zeta(t) = \text{Re}[\zeta_0(\omega)e^{i\omega t}]$, where $\zeta_0(\omega) = \zeta'_0(\omega) - i\zeta''_0(\omega)$. Then $\zeta'_0(\omega) = \hat{\zeta}_0(\omega)\cos\delta(\omega)$, $\zeta''_0(\omega) = -\hat{\zeta}_0(\omega)\sin\delta(\omega)$, and thus $\hat{\zeta}_0(\omega) \equiv |\zeta_0(\omega)|$. The complex mechanical susceptibility is defined as

$$\chi(\omega) = \chi'(\omega) - \chi''(\omega) = \frac{\zeta_0(\omega)}{f_0} \quad (6)$$

and obviously $\chi'(\omega) = \hat{\zeta}_0(\omega)\cos\delta(\omega)/f_0$, $\chi''(\omega) = \hat{\zeta}_0(\omega)\sin\delta(\omega)/f_0$, which implies the well-known relation $\chi''(\omega)/\chi'(\omega) = \tan\delta(\omega)$. The preceding formulas yield the following central relation between $\chi''(\omega)$ and the average mechanical work done on the system:

$$\chi''(\omega) = \frac{2}{\omega f_0^2} \left\langle \frac{dE_m}{dt} \right\rangle. \quad (7)$$

Since the real part $\chi'(\omega)$ is determined by the Kramers-Kronig relation, the compliance $S_{kk}(\omega)$ can therefore be calculated from Eq. (4) once $\langle dE_m/dt \rangle$ is known.

Dynamic elastic measurements are usually performed by recording the response of a parallelepiped-shaped crystal to either uniaxial compression or bending. Here we treat the most important practical cases of compression between parallel plates and midbending between two supports.

In the so-called parallel plate mode (PPM), the force f acts on the part $O_1 := l_2 \times l_3$ of the volume $V = l_1 \times l_2 \times l_3$. Then obviously $\sigma_1 = f/O_1$ is the only nonvanishing stress component in the volume, which induces strains $\epsilon_i = S_{i1}^T f/O_1$. The elongation ζ corresponding to f is therefore

$$\zeta = l_1 \epsilon_1 = \frac{l_3^2}{3} f_0 S_{11}^T. \quad (8)$$

In the three-point bending (3PB) mode things are slightly less trivial. In fact, consider a horizontal stick of length l with rectangular profile A . We choose x as the length coordinate $-l/2 < x < l/2$ along the stick's horizontal axis. Suppose now that the stick is freely supported on its edges and weakly bent by a force $f \equiv (0, 0, -f)$ acting on the stick's upper surface on the line $x=0$ parallel to the axis z . When bending, a part of the volume will be compressed and another part will be dilated, while on a whole plane, the so-called neutral fiber, no compression or dilatation occurs. Let $-d/2 < z < d/2$ denote the vertical axis, i.e., the stick's thickness coordinate with respect to the neutral fiber, and y the remaining width coordinate. Then, the vertical displacement of the neutral fiber follows the weak bending formula¹⁰

$$\zeta(x) = \frac{f}{48EI} (l^3 - 6lx^2 + 4|x|^3) \quad -l/2 \leq x \leq l/2, \quad (9)$$

where $E = E_{xx}$ denotes the corresponding elastic module in direction x . $I = \int_A z^2 dz dy$ is the area momentum of A with

respect to the y axis perpendicular to x, z . In particular, the maximum displacement at $x=0$ is

$$\zeta_{\max} = \frac{fl^3}{48EI}. \quad (10)$$

This implies that a bending resulting in a displacement z of the stick's center $(0, 0, 0)$ follows the relation $f = kz$ with spring constant $k = 48EI/l^3$. A short calculation shows that the mechanical energy stored in bending is

$$E_m = \frac{k}{2} \zeta_{\max}^2 \equiv \frac{EI}{2} \int_{-l/2}^{l/2} dx [\zeta''(x)]^2 = \frac{1}{2} \int_V dV [z\zeta''(x)][Ez\zeta''(x)]. \quad (11)$$

In the treated case of weak bending only $\sigma_1(\mathbf{x}) \equiv \sigma_{xx}(\mathbf{x}) \neq 0$ (cf. Ref. 10). Therefore, comparison with the general formula $E_m = \frac{1}{2} \int_V dV \sum_i \epsilon_i(\mathbf{x}) \sigma_i(\mathbf{x})$ yields the manifestly inhomogeneous stress-strain distribution

$$\epsilon_1(\mathbf{x}) = z\zeta''(x), \quad \sigma_1(\mathbf{x}) = E\epsilon_1(\mathbf{x}) = Ez\zeta''(x). \quad (12)$$

Since $\zeta''(x) = f/48EI(24|x| - 12l)$, we finally obtain

$$\epsilon_1(\mathbf{x}) = \frac{f}{3EI}(2|x| - l)z, \quad \sigma_1(\mathbf{x}) = \frac{f}{3I}(2|x| - l)z. \quad (13)$$

III. FUNDAMENTAL EQUATIONS OF HEAT DIFFUSION

Suppose now that the system is in contact with a heat bath of temperature \bar{T} . Switching on the weak periodic external force $f(t)$ will produce a small stress field $\sigma_i = \sigma_i(t, \mathbf{r})$. Let $G(\bar{T}, \boldsymbol{\sigma})$ denote the corresponding Gibbs free energy. The stress σ_i in turn induces infinitesimal strains $\epsilon_i(T, \mathbf{r}) = (\partial G / \partial \sigma_i)_T$ as well as small temperature changes $\delta T = \delta T(t, \mathbf{r})$ in the system. This leads to a small inhomogeneous heat distribution

$$\delta Q(t, \mathbf{r}) \approx C_\sigma \delta T(t, \mathbf{r}) + \bar{T} \sum_i \left(\frac{\partial S}{\partial \sigma_i} \right)_T \sigma_i(t, \mathbf{r}), \quad (14)$$

where $C_\sigma = \bar{T}(\partial \bar{S} / \partial \bar{T})_{\bar{\boldsymbol{\sigma}}}$ denotes the specific heat at constant stress $\bar{\boldsymbol{\sigma}}$. We introduce the *thermal-expansion* coefficients $\alpha_i := (\partial \bar{\epsilon} / \partial \bar{T})_{\bar{\boldsymbol{\sigma}}} = -[\partial \bar{S} / \partial \sigma_i(\mathbf{r})]_{\bar{T}}$. Then $\delta Q(t, \mathbf{r}) = C_\sigma \delta T(t, \mathbf{r}) - \bar{T} \sum_i \alpha_i \sigma_i(t, \mathbf{r})$, which implies

$$\frac{\partial Q(t, \mathbf{r})}{\partial t} = C_\sigma \frac{\partial T(t, \mathbf{r})}{\partial t} - \bar{T} \sum_i \alpha_i \frac{\partial \sigma_i(t, \mathbf{r})}{\partial t}. \quad (15)$$

Combining this with the heat equation

$$\frac{\partial Q(t, \mathbf{r})}{\partial t} = \kappa \Delta_r T(t, \mathbf{r}) \quad (16)$$

we arrive at the linear partial differential equation

$$\frac{\partial U(t, \mathbf{r})}{\partial t} - D \Delta_r U(t, \mathbf{r}) = F(t, \mathbf{r}) \quad (17)$$

for the temperature fluctuation $U(t, \mathbf{r}) := T(t, \mathbf{r}) - \bar{T}$, where $D := \kappa/C_\sigma$ is the *thermal diffusivity*, and

$$F(t, \mathbf{r}) := \frac{\bar{T}}{C_\sigma} \sum_i \alpha_i \frac{\partial \sigma_i(t, \mathbf{r})}{\partial t} \quad (18)$$

will be called the *thermal driving function* (TDF) in the following. Suppose now that the external force $f(t)$ of period $2\pi/\omega$ is switched on at $t=0$. After the initial configuration $U_0(\mathbf{r})$ has died out, a periodically oscillating temperature distribution $T(t, \mathbf{r}) = \bar{T} + U(t, \mathbf{r})$ will be found in the system, which induces the heat current $\mathbf{q}(\mathbf{x}) = -\kappa \nabla T(\mathbf{r}) = -\kappa \nabla U(\mathbf{r})$. Making use of the heat equation (16), the resulting entropy loss per unit time is

$$\begin{aligned} \frac{dS}{dt} &= - \int_V dV \frac{\nabla \mathbf{q}}{T} = - \int_V dV \left[\nabla \left(\frac{\mathbf{q}}{T} \right) - \mathbf{q} \cdot \nabla \left(\frac{1}{T} \right) \right] \\ &= \underbrace{\kappa \int_O \frac{d\mathbf{f} \cdot \nabla U}{T}}_{(1)} + \underbrace{\kappa \int_V dV \frac{(\nabla U)^2}{T^2}}_{(2)}, \end{aligned} \quad (19)$$

where Gauss's theorem was used. We now expand $1/T = (1/\bar{T}) - (U/\bar{T}^2) + O(U^2)$. Then to order $O(U^3)$, again using Gauss's theorem, we obtain the two contributions

$$(1) = - \frac{\kappa}{\bar{T}^2} \int_O d\mathbf{f} \cdot (\nabla U) U, \quad (20a)$$

$$(2) = \frac{\kappa}{\bar{T}^2} \int_O d\mathbf{f} \cdot (\nabla U) U - \frac{\kappa}{\bar{T}^2} \int_V dV U \Delta U. \quad (20b)$$

Altogether, since $dE_m/dt = \bar{T} dS/dt$, this yields

$$\frac{dE_m}{dt} = \frac{\kappa}{\bar{T}} \int_V dV U (-\Delta) U + O(U^3) \quad (21)$$

and so, averaged over one period,

$$\left\langle \frac{dE_m}{dt} \right\rangle = \frac{\omega}{2\pi} \int_0^{2\pi/\omega} dt \left[\frac{\kappa}{\bar{T}} \int_V dV U (-\Delta) U \right]. \quad (22)$$

IV. SOLUTION FOR A PARALLELEPIPED

A. Analysis of boundary conditions

An analysis of Eq. (22) is quite essential for understanding the nature of heat diffusion. In fact, the two contributions (20a) and (20b) represent the mechanical energy loss dE_m/dt resulting from heat dissipation through the surface O as well as heat transfer between different regions within the crystal. Adding these contributions, the surface terms seem to cancel. Nevertheless the admissible eigenvalues of the Laplacian $(-\Delta)$ crucially depend on the boundary conditions imposed on its eigenfunctions, actually leaving the problem undefined unless we fix them. In this aspect, a consistent treatment of heat diffusion takes a lot more care than many other phase-transition-related problems, where it is usually safe to assume that the bulk effect is orders-of-

magnitude larger than surface contributions and therefore any choice of boundary conditions will do. Indeed, in the literature various types of boundary conditions have been imposed in a more or less justified way.

- Chaves *et al.*⁴ assume that the crystal's surface is in perfect contact with an infinite medium of the same thermal conductivity κ . To what extent this is physically relevant will be discussed below.
- Fally *et al.*⁷ consider isothermal boundary conditions, i.e., they take κ to be infinite on the crystal's surface O . While this may be reasonable in a dielectric context where the crystal's surface is vaporized with metal for measurements, there is no point in introducing such an assumption for elastic measurements. Yet, in the presence of domains, the resulting boundary conditions will turn out to be of considerable relevance.
- In a surrounding vacuum, finite heat loss is due to radiation and could be described by the Stefan-Boltzmann law, i.e., it is proportional to T .⁴
- In the elastic context, convection will provide the most important contribution in the presence of purge gas or air, where finite heat conduction on the surface is mainly caused by free and forced convection.

In what follows we will focus on the case of heat loss due to convection. To account for this, we employ Newton's law of heat conduction, which states that heat transfer on the surface is proportional to the heat difference of the surface and its surroundings. In other words, recalling that $\mathbf{q} = -\kappa \nabla_r T = -\kappa \nabla_r U$, we impose the boundary conditions

$$[\mathbf{n} \cdot \nabla_r U(t, \mathbf{r}) + hU(t, \mathbf{r})]_{r \in O} = 0, \quad (23)$$

where \mathbf{n} denotes the outer surface normal vector and h is known as the heat transfer coefficient.

B. Admissible base functions

We now consider a specimen of volume $V = l_1 \times l_2 \times l_3$. Then it is convenient to define the dimensionless vectors $\mathbf{x} \in \hat{V} := [-1/2, 1/2]^3$ by setting $x_i := r_i/l_i$. We also introduce the coefficients $D_i := D/l_i^2$ and the dimensionless parameters $\gamma_i := l_i h$. Then we can restate Eqs. (17) and (23) as the system of inhomogeneous partial differential equations

$$\frac{\partial u(t, \mathbf{x})}{\partial t} + Lu(t, \mathbf{x}) = \hat{F}(t, \mathbf{x}), \quad L := - \sum_{i=1}^3 D_i \frac{\partial^2}{\partial x_i^2}, \quad (24)$$

with initial condition $u(0, \mathbf{x}) = u_0(\mathbf{x})$ and boundary conditions

$$\frac{\partial u(t, \mathbf{x})}{\partial x_i} \pm \gamma_i u(t, \mathbf{x}) = 0, \quad x_i = \pm 1/2, \quad (25)$$

where $u(t, \mathbf{x}) \equiv U[t, (l_i x_i)]$, $u_0(\mathbf{x}) \equiv U_0[(l_i x_i)]$, $\hat{\sigma}_i(t, \mathbf{x}) \equiv \sigma_i[t, (l_i x_i)]$, and $\hat{F}(t, \mathbf{x}) \equiv F[t, (l_i x_i)]$. The energy dissipation per volume is then written as

$$\frac{1}{V} \frac{dE_m}{dt} = \frac{C\sigma}{\bar{T}} \int_{\hat{V}} d^3x u L u. \quad (26)$$

The solution of the system of Eqs. (24) and (25) can be constructed using the eigenfunctions $N_e(q_i)\cos(q_i x_i)$, $N_o(q_i)\sin(p_j x_j)$ of the elliptic operator $-\partial^2/\partial x_i^2$ defined on the interval $[-1/2, 1/2]$. The factors

$$N_e(q_i) := \sqrt{\frac{2q_i}{q_i + \sin q_i}}, \quad N_o(q_i) := \sqrt{\frac{2p_j}{p_j - \sin p_j}} \quad (27)$$

are chosen to normalize these functions to 1 with respect to the L_2 Hilbert-space norm. As they are subject to the boundary conditions (25), possible wave vectors \mathbf{p}, \mathbf{q} must satisfy the relations

$$\cot \frac{q_i}{2} = + \frac{q_i}{\gamma_i}, \quad \tan \frac{p_j}{2} = - \frac{p_j}{\gamma_j}. \quad (28)$$

These equations allow for an infinite number of solutions $q_i(m_i)$, $p_j(m_j)$, $m_i, m_j = 0, 1, 2, \dots$, corresponding to the admissible wave numbers in directions i and j , respectively, yielding the admissible wave vectors $\mathbf{q}(\mathbf{n}) := [q_1(m_1), q_2(m_2), q_3(m_3)]$, $\mathbf{p}(\mathbf{m}) := [p_1(m_1), p_2(m_2), p_3(m_3)]$. We parametrize the solutions $q_i(m_i)$, $p_j(m_j)$, of Eq. (28) by

$$q_i(m_i) = \hat{q}_i(m_i) + 2\pi m_i, \quad (29a)$$

$$p_j(m_j) = \hat{p}_j(m_j) + 2\pi m_j, \quad m_i, m_j = 0, 1, 2, \dots, \quad (29b)$$

where $\hat{q}_i(m_i), \hat{p}_j(m_j)$ satisfy the relations

$$\cot \frac{\hat{q}_i(m_i)}{2} = \frac{\hat{q}_i(m_i) + 2\pi m_i}{\gamma_i}, \quad (30a)$$

$$\tan \frac{\hat{p}_j(m_j)}{2} = - \frac{\hat{p}_j(m_j) + 2\pi m_j}{\gamma_j} \quad (30b)$$

since $\cot(x+m\pi) = \cot x$, and $\tan(x+m\pi) = \tan x$. For general values of γ_i these equations can only be solved numerically. Notice, however, that since $\tan[(x-\pi)/2] = -\cot(x/2)$, we have

$$p_j(m_j) \equiv q_j\left(\frac{2m_j-1}{2}\right). \quad (31)$$

In particular, since $\cot \pi/2 = 0$, we obtain $\hat{q}_j(-1/2) = \pi$, yielding $\hat{p}_j(0) = 0$. Summarizing these relations, for $0 < h < \infty$ and any $\mathbf{n} \in \mathbb{N}_0^3$ there is a base function $f_{\mathbf{n}}(\mathbf{x}) := \prod_{i=1}^3 f_{n_i}(x_i)$ defined by

$$f_{n_i}(x_i) := \begin{cases} N_e[q_i(n_i/2)] \cos[q_i(n_i/2)x_i] & n_i \text{ even,} \\ N_o[q_i(n_i/2)] \sin[q_i(n_i/2)x_i] & n_i \text{ odd.} \end{cases} \quad (32)$$

Each such function is an eigenfunction for the Laplacian $-\Delta$ with eigenvalue $\sum_{i=1}^3 q_i^2(n_i/2)$, but simultaneously also for the operator L with eigenvalue

$$\lambda_{\mathbf{n}} := \sum_{i=1}^3 D_i q_i^2(n_i/2). \quad (33)$$

It is shown in Refs. 11 and 12 that these functions form a complete orthonormal base of the Hilbert space $L_2(\hat{V}, \mathbb{R})$ for set of $\gamma_1, \gamma_2, \gamma_3 > 0$. Obviously $q_i(0) < q_i(1/2) < q_i(1) < q_i(3/2) < q_i(2) < \dots$, and since $q_i(0) > 0$ for $0 < h < \infty$, we conclude that *all eigenvalues $\lambda_{\mathbf{n}}$ are positive*. The following limiting cases are of particular interest:

- $\gamma_i \rightarrow \infty$ (isothermal boundary conditions along direction i). Then $u(t, \mathbf{x}) \equiv 0$ for $x_i = \pm 1/2$ and since $\gamma_i \rightarrow \infty$, we have $\cot \hat{q}_i(n_i/2)/2 = 0$, which implies that $\lim_{\gamma_i \rightarrow \infty} \hat{q}_i(n_i/2) = \pi$ and consequently $\lim_{h \rightarrow \infty} q_i(n_i/2) = (n_i + 1)\pi > 0 \forall n_i \geq 0$. All eigenvalues $\lambda_{\mathbf{n}}$ are positive and

$$f_{n_i}(x_i) = \sqrt{2} \times \begin{cases} \cos[(n_i + 1)\pi x_i] & n_i \text{ even,} \\ \sin[(n_i + 1)\pi x_i] & n_i \text{ odd.} \end{cases} \quad (34)$$

- $\gamma_i \ll 1$ (almost adiabatic boundary conditions). We note the series expansions

$$N_e(0) = 1 + \frac{\gamma_i}{12} + O(\gamma_i^2), \quad (35a)$$

$$q_i(0) = \sqrt{2}\gamma_i - \frac{\gamma_i^{3/2}}{6\sqrt{2}} + O(\gamma_i^{5/2}) \quad (35b)$$

and

$$q_i(n_i) = 2\pi n_i + \frac{\gamma_i}{\pi n_i} - \frac{\gamma_i^2}{2n_i^3 \pi^3} + O(\gamma_i^3), \quad (36a)$$

$$N_{e,o}(n_i) = \sqrt{2} \left(1 - \frac{\gamma_i}{n_i^2 \pi^2} \right) + O(\gamma_i^2), \quad (36b)$$

which imply that $\lim_{\gamma_i \rightarrow 0} q_i(n_i/2) = n_i \pi$, $n_i = 0, 1, 2, \dots$. Thus, in the limiting case $\gamma_i = 0$ we obtain

$$f_{n_i}(x_i) = \sqrt{2} \times \begin{cases} \cos[n_i \pi x_i] & n_i \text{ even,} \\ \sin[n_i \pi x_i] & n_i \text{ odd.} \end{cases} \quad (37)$$

Thus, only under the hypothetic assumption $h = 0$ of perfect thermal isolation on the complete surface O would the constant function $f(x) \equiv 1/V$ with corresponding eigenvalue $\lambda_0 = 0$ be admissible. Numerically, a noticeable adiabatic-to-isothermal crossover occurs for approximately $1 \approx \gamma_i^{\text{adiabat}} < \gamma_i < \gamma_i^{\text{iso}} \approx 500$.

C. General solution for periodic external force

According to Fourier's method of solving partial differential equations, one can show that using the projection coefficients

$$a^n := \int_{\hat{V}} d^3x f_{\mathbf{n}}(\mathbf{x}) u_0(\mathbf{x}), \quad (38a)$$

$$c^n(s) := \int_{\hat{V}} d^3x f_n(\mathbf{x}) \hat{F}(s, \mathbf{x}) \quad (38b)$$

any solution of Eq. (24) for a given TDF $\hat{F}(t, \mathbf{x})$ and initial configuration $u_0(\mathbf{x})$ can be expanded in terms of the base functions $f_n(\mathbf{x})$ as

$$u(t, \mathbf{x}) = \sum_{n \in \mathbb{N}_0^3} e^{-\lambda_n t} \left[a^n + \int_0^t ds c^n(s) e^{\lambda_n s} \right] f_n(\mathbf{x}). \quad (39)$$

For later use, we define the relaxation times $\tau_n := 1/\lambda_n$ and the spatial averages $\bar{f}_n := \int_{\hat{V}} d^3x f_n(\mathbf{x})$. Obviously $\bar{f}_n = 0$ if just one n_i happens to be odd.

We now consider a stress field $\hat{\sigma}_i(t, \mathbf{x}) = \hat{\sigma}_i^0(\mathbf{x}) \cos(\omega t)$ periodic in time. This yields a TDF

$$\hat{F}(t, \mathbf{x}) = \frac{\bar{T}}{C_\sigma} \sum_i \alpha_i \hat{\sigma}_i^0(\mathbf{x}) [-\omega \sin(\omega t)] \quad (40)$$

with a spatial part

$$\hat{F}^0(\mathbf{x}) := \frac{\bar{T}}{C_\sigma} \sum_i \alpha_i \hat{\sigma}_i^0(\mathbf{x}). \quad (41)$$

After the memory of the initial configuration $u_0(\mathbf{x})$ has died out, $u(t, \mathbf{x})$ will be shown below to be of the general form

$$u(t, \mathbf{x}) = \sum_{n \in \mathbb{N}_0^3} u_n(t) f_n(\mathbf{x}). \quad (42)$$

The energy dissipation per volume is [cf. Eq. (26)]

$$\frac{1}{V} \frac{dE_m}{dt} = \frac{C_\sigma}{\bar{T}} \int_{\hat{V}} d^3x u L u = \frac{C_\sigma}{\bar{T}} \sum_{n \in \mathbb{N}_0^3} u_n^2(t) \lambda_n, \quad (43)$$

where the orthonormality of the base functions $f_n(\mathbf{x})$ was used. Therefore, the average energy dissipation is

$$\frac{1}{V} \left\langle \frac{dE_m}{dt} \right\rangle = \frac{C_\sigma}{\bar{T}} \sum_{n \in \mathbb{N}_0^3} \left[\frac{\omega}{2\pi} \int_0^{2\pi/\omega} dt u_n^2(t) \right] \lambda_n, \quad (44)$$

which implies for $\chi''(\omega) = (2/\omega f_0^2) 1/V \langle dE_m/dt \rangle$ the general formula

$$\chi''(\omega) = \frac{C_\sigma}{\bar{T} f_0^2} \sum_{n \in \mathbb{N}_0^3} \lambda_n \frac{1}{\pi} \int_0^{2\pi/\omega} dt u_n^2(t). \quad (45)$$

At this stage it is already obvious that $\lim_{\omega \rightarrow \infty} \chi''(\omega) = 0$. We now calculate the functions $u_n(t)$. The coefficients $c^n(s)$ are

$$c^n(s) = [-\omega \sin(\omega s)] \frac{\bar{T}}{C_\sigma} \sum_i \alpha_i \hat{\sigma}_{in}^0, \quad (46)$$

where

$$\hat{\sigma}_{in}^0 = \int_{[-1/2, 1/2]^3} d^3x f_n(\mathbf{x}) \hat{\sigma}_i^0(\mathbf{x}), \quad (47)$$

and so

$$e^{-\lambda_n t} \int_0^t ds c^n(s) e^{\lambda_n s} = -\frac{\bar{T}}{C_\sigma} \frac{\omega}{\lambda_n^2 + \omega^2} [\omega e^{-\lambda_n t} - \omega \cos(\omega t) + \lambda_n \sin(\omega t)] \left(\sum_i \alpha_i \hat{\sigma}_{in}^0 \right). \quad (48)$$

Therefore,

$$u(t, \mathbf{x}) = \sum_{n \in \mathbb{N}_0^3} e^{-\lambda_n t} a^n f_n(\mathbf{x}) - \frac{\bar{T}}{C_\sigma} \sum_{n \in \mathbb{N}_0^3} \frac{\omega}{\lambda_n^2 + \omega^2} [\omega e^{-\lambda_n t} - \omega \cos(\omega t) + \lambda_n \sin(\omega t)] \left(\sum_i \alpha_i \hat{\sigma}_{in}^0 \right) f_n(\mathbf{x}), \quad (49)$$

from which we extract

$$u_n(t) = -\frac{\bar{T}}{C_\sigma} \frac{\omega}{\lambda_n^2 + \omega^2} [-\omega \cos(\omega t) + \lambda_n \sin(\omega t)] \left(\sum_i \alpha_i \hat{\sigma}_{in}^0 \right) \quad (50)$$

for $0 < \gamma_i < \infty$ in the limes $t \gg 1$. From this we obtain

$$\frac{1}{\pi} \int_0^{2\pi/\omega} dt u_n^2(t) = \frac{\omega}{\lambda_n^2 + \omega^2} \frac{\bar{T}^2}{C_\sigma^2} \left(\sum_i \alpha_i \hat{\sigma}_{in}^0 \right)^2. \quad (51)$$

According to Eq. (45), this finally yields

$$\chi''(\omega) = \frac{1}{f_0^2} \sum_{n \in \mathbb{N}_0^3} \frac{\omega \lambda_n}{\lambda_n^2 + \omega^2} \left(\sum_i \alpha_i \hat{\sigma}_{in}^0 \right)^2. \quad (52)$$

This is a sum of negative imaginary parts of Debye-like contributions $\propto \lambda_n / (\lambda_n + i\omega) = 1/(1 + i\omega\tau_n)$. The full complex susceptibility must therefore be of the form

$$\begin{aligned} \chi(\omega) &= \chi_\infty + \frac{1}{f_0^2} \sum_{n \in \mathbb{N}_0^3} \frac{\left(\sum_i \alpha_i \hat{\sigma}_{in}^0 \right)^2}{1 + i\omega\tau_n} \\ &= \chi_\infty + \frac{1}{f_0^2} \sum_{n \in \mathbb{N}_0^3} \frac{\left(\sum_i \alpha_i \hat{\sigma}_{in}^0 \right)^2}{1 + i\omega\tau_n} \end{aligned} \quad (53)$$

Specializing to uniaxial pressure in direction k , i.e., $\hat{\sigma}_i^0(\mathbf{x}) = 0$, $i \neq k$, the high-frequency limit $\chi_\infty \in \mathbb{R}$ is determined as follows. In view of Eq. (4) we identify

$$S_{kk}(\omega) \equiv \frac{f_0^2}{\|\sigma_k\|_{L_2}^2} \chi(\omega) = \frac{f_0^2}{\|\hat{\sigma}_k^0\|_{L_2}^2} \chi_\infty + \frac{\bar{T} \alpha_k^2}{C_\sigma} \Omega(\omega), \quad (54)$$

where we introduce the crossover function

$$\Omega(\omega) := \frac{1}{\|\hat{\sigma}_k^0\|_{L_2}^2} \sum_{n \in \mathbb{N}_0^3} \frac{(\hat{\sigma}_{kn}^0)^2}{1 + i\omega\tau_n}. \quad (55)$$

Notice that this can also be written as

$$\Omega(\omega) = \frac{1}{\|\hat{F}^0\|_{L_2}^2} \sum_{n \in \mathbb{N}_0^3} \frac{(\hat{F}_n^0)^2}{1 + i\omega\tau_n} \quad (56)$$

since in the present situation $\hat{\sigma}_k^0(\mathbf{x})$ is proportional to $\hat{F}^0(\mathbf{x})$ [cf. Eq. (41)]. Using the completeness of eigenfunctions we calculate the limits

$$\lim_{\omega \rightarrow 0} \Omega(\omega) = \frac{1}{\|\hat{\sigma}_k^0\|_{L_2}^2} \sum_{n \in \mathbb{N}_0^3} (\hat{\sigma}_{kn}^0)^2 = 1, \quad (57a)$$

$$\lim_{\omega \rightarrow \infty} \Omega(\omega) = 0. \quad (57b)$$

This allows to express the complex elastic compliance $S_{kk}(\omega)$ by the adiabatic and isothermal compliances

$$S_{kk}^S := \lim_{\omega \rightarrow \infty} S_{kk}(\omega) \equiv \frac{f_0^2}{\|\hat{\sigma}_k^0\|_{L_2}^2} \chi_\infty, \quad (58a)$$

$$S_{kk}^T := \lim_{\omega \rightarrow 0} S_{kk}(\omega) \equiv S_{kk}^S + \frac{\bar{T}\alpha_k^2}{C_\sigma} \quad (58b)$$

as

$$S_{kk}(\omega) = S_{kk}^S + (S_{kk}^T - S_{kk}^S)\Omega(\omega), \quad (59)$$

from which instantly deduce the elastic Pippard relation

$$S_{kk}^T - S_{kk}^S = \frac{\bar{T}\alpha_k^2}{C_\sigma}. \quad (60)$$

Formulas (59) and (55) are the fundamental equations for discussing heat-diffusion phenomena. The physical content of Eq. (55) is quite transparent. Each spatial projection coefficient $\hat{\sigma}_{kn}^0$ onto the corresponding heat conduction mode $f_n(\mathbf{x})$ contributes a Debye-like relaxation propagating with relaxation time τ_n , which is determined by the heat conduction coefficient, the specific heat, and the boundary conditions. The amplitude of the whole effect is proportional to α_k^2 . It will therefore be most likely observed in the vicinity of a phase transition. The Pippard relation (60) is recognized as a simple consequence of the completeness of the system of eigenfunctions $f_n(\mathbf{x})$ and energy conservation.

We emphasize that in contrast to former treatments (cf. Refs. 4, 5, 7, and 8), Eqs. (55) and (59) do not explicitly depend on any particular assumptions concerning the spatial nature of the excitation or the boundary conditions on the surface of the sample. Therefore we feel that they are suitable for a general discussion of heat-diffusion phenomena. In particular, the present theory holds for arbitrary spatial de-

pendence of the TDF $\hat{F}(t, \mathbf{x}) \propto \alpha_k \hat{\sigma}_k(\mathbf{x})$ generated by the external force f . Such spatial inhomogeneities can, in principle, arise due to different reasons:

- The stress distribution $\hat{\sigma}_k(\mathbf{x})$ may be inhomogeneous as a result of the action of the external force f itself, such as the case in a 3PB experiment.
- One can also introduce a spatial dependence $\alpha_k(\mathbf{x})$ of α_k . Assuming $\hat{\sigma}_k^0(\mathbf{x}) = \text{const}$ to be homogeneous but taking $\alpha_k(\mathbf{x}) = \pm |\alpha_k|$ is obviously equivalent to a situation where $\alpha_k = \text{const}$ while $\hat{\sigma}_k(\mathbf{x}) = \pm |\hat{\sigma}_k^0|$. This can be used to study the contributions originating purely from heat diffusion, i.e., in a crystal with an completely regular domain pattern.

Since Eq. (55) represents an infinite sum of Debye-like contributions with different relaxation times, the resulting crossover function is non-Debye in principle, and in fact, several of the crossover functions found in the cited references from a variety of theoretical assumptions are of a corresponding nature. However, it remains to investigate under which experimental conditions non-Debye-like behavior is actually expected to be manifestly observed in a *real* experiment.

V. HEAT DIFFUSION IN MONODOMAIN CRYSTALS

A. PPM experiments

1. General solution

In a PPM, where the uniaxial stress σ_k^0 is homogeneous, the only nonzero projection coefficients are determined from

$$\frac{(\hat{\sigma}_{k2m}^0)^2}{\|\hat{\sigma}_k^0\|_{L_2}^2} = \left[\int_{\hat{V}} d^3x \mathbf{1} \cdot f_{2m}(\mathbf{x}) \right]^2 = \bar{f}_{2m}^2. \quad (61)$$

This yields the PPM crossover function

$$\Omega(\omega) = \sum_{m \in \mathbb{N}_0^3} \frac{\bar{f}_{2m}^2}{1 + i\omega\tau_{2m}}. \quad (62)$$

In the following we are interested in the dependence of $\Omega(\omega)$ on the dimensionless parameters $\gamma_i = hl_i$ determined by the sample geometry and the boundary conditions. However, in three dimensions, most calculations can only be evaluated numerically. Since the results below remain qualitatively valid in three dimensions, some analytic illustrations obtained for $d=1$ are therefore presented, which is a useful and admissible simplification for the case of platelike samples of small thickness frequently encountered in experiment. To compare the behavior of different crossover functions it is convenient to investigate their corresponding Cole-Cole plots. Recall that the Cole-Cole (CC) plot of a complex-valued function $\Omega(\omega) = \Omega'(\omega) - i\Omega''(\omega)$, $\omega > 0$ is defined as the ω -parametrized function graph $\{(\Omega'(\omega), \Omega''(\omega)), \omega > 0\}$. Inspecting formula (55), we notice that ω always enters through the product

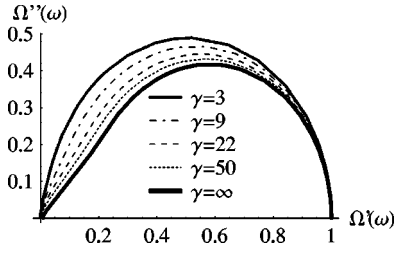


FIG. 1. CC plot of the one-dimensional crossover function $\Omega(\omega)$ for dimensionless parameter $\gamma=3, 9, 22, 50$, and ∞ .

$$\omega\tau_n = \frac{\omega}{D} \left[\sum_{i=1}^3 q_i^2(n_i/2)/l_i^2 \right]^{-1}. \quad (63)$$

Since $D^{-1} = D^{-1}(T) = C_\sigma(T)/\kappa(T)$ usually displays a considerable anomaly in the vicinity of T_c , we conclude that the CC plot of a heat-diffusion crossover function $\Omega(\omega)$ can equally be parametrized by either angular frequency ω at fixed temperature T or temperature T at a fixed value of angular frequency ω .

Now it is well known that the CC plot of a Debye-like function $\Omega(\omega) \sim 1/(1+i\omega\tau)$, $\tau > 0$ represents an upper half circle in the complex plane. As shown in Fig. 1, for growing values of γ_i , the non-Debye characteristics of $\Omega(\omega)$ become increasingly manifest as the CC plot of $\Omega(\omega)$ becomes more and more asymmetric. However, one should consider the following quantitative estimates.

In a usual PPM experiment, specimen are of sizes of order $l_i \sim 1$ cm. On the other hand, the parameter h depends on various quantities, which are experimentally difficult to control. For example, in the case of forced convection due to the use of purge gas, h depends on parameters such as purge gas density and velocity, purge flow geometry, turbulence effects, and so on. However, inspecting the literature,¹³ one finds that realistic values of h for forced convection are confined to a region $h < 10$ cm⁻¹, yielding $\gamma_i < 10$. For free convection, h is yet orders of magnitude smaller. Bearing in mind that the Debye factor $1/[1+i\omega\tau_{q(2m)}]$ rapidly approaches zero for growing values of m_i , a numerical investigation of the factors $f_{2m_i}^2$ as a function of γ_i (see Fig. 2) reveals the fact that for usual experimental conditions only the term $m=0$ gives a significant contribution to $\Omega(\omega)$.

For $\gamma_i \ll 1$, we collect the expansions

$$q_i(0) = \sqrt{2}\gamma_i + O(\gamma_i^{3/2}), \quad q_i(2m_i) = \frac{\gamma_i}{\pi m_i} + O(\gamma_i^2) \quad (64)$$

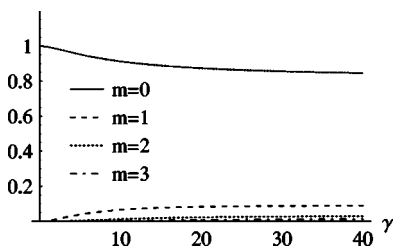


FIG. 2. Coefficients f_{2m}^2 as a function of γ for $m=0-3$.

($n_i=1,2,3, \dots$) yielding

$$\lambda_0 = 2 \sum_{i=1}^3 D_i \gamma_i + O(\gamma_i^2) = 2Dh \sum_{i=1}^3 \frac{1}{l_i} + O[(hl_i)^2]. \quad (65)$$

For the realistic case $\gamma_i \ll 1$ we can therefore conclude that the infinite sum of Eq. (55) actually collapses to give a Debye-like dispersion $\Omega(\omega) \sim 1/(1+i\omega\tau_0)$ with relaxation time

$$\tau_0 \sim \left(2Dh \sum_{i=1}^3 \frac{1}{l_i} \right)^{-1} = \frac{1}{Dh} \frac{V}{O}. \quad (66)$$

As far as single domain crystals are concerned, we are not aware of any clear detection of elastically induced heat diffusion using a PPM measurement nor of a corresponding observation in a dielectric experiment. However, let us compare the above predictions to the result of quite recent⁹ PPM measurements of temperature and frequency dependencies of the complex elastic susceptibility of KMnF_3 . Indeed, in pure KMnF_3 an ultraslow relaxational process just below the structural phase transition at $T_c = 186$ K was discovered (Fig. 3), and as the inset of Fig. 3 shows, the CC plot of the data points is in reasonably good agreement with a Debye half circle as expected from Eq. (66). Unfortunately, due to the comparatively wide distribution of measurement points, these data are not absolutely conclusive. A closer experimental investigation using frequency scans at fixed temperatures is in progress.

2. Isothermal boundary conditions

In $d=1$ dimensions the crossover function can be calculated in a closed form for isothermal boundary conditions. In fact, letting $\gamma_1 \rightarrow \infty$ then yields $\tau_{2m} = (1/D_1 \pi^2) 1/(2m+1)^2$, $m=0,1,2, \dots$, $f_{2m}(x) = \sqrt{2} \cos[(2m+1)\pi x]$ and so $f_{2m}^2 = (8/\pi^2) 1/(2m+1)^2$. The resulting infinite sum can be explicitly performed and yields the $d=1$ crossover function of Fally *et al.*,⁷

$$\Omega_{\text{Fally}}^{(d=1)}(\xi) = \frac{(1+i)}{\sqrt{\xi}} \tan \left[\frac{(1-i)}{2} \sqrt{\xi} \right], \quad \xi = \frac{\omega}{2D_1}. \quad (67)$$

The negative imaginary part $\Omega_{\text{Fally}}^{(d=1)''}(\xi)$ peaks at $\xi = 5.08129$, leading to a typical relaxation time of order

$$\tau_{\text{Fally}} \approx \frac{1}{5 \times 2D_1} = \frac{l_1^2}{10D}. \quad (68)$$

In Ref. 7, these results were obtained in a dielectric context, where the use of isothermal boundary conditions may be justified as we mentioned above. In contrast, for typical elastic PPM experiments on monodomain samples such boundary conditions are clearly ruled out. However, we chose to record the ($d=1$) dispersion function (67) here because it is of considerable interest in discussing the polydomain case below.

For dimensions $d=2,3$ the resulting dispersion can only be evaluated numerically. A CC plot of $\Omega_{\text{Fally}}^{(d)}(\xi)$ for isothermal boundary conditions in $d=1,2,3$ is presented in Fig. 4.

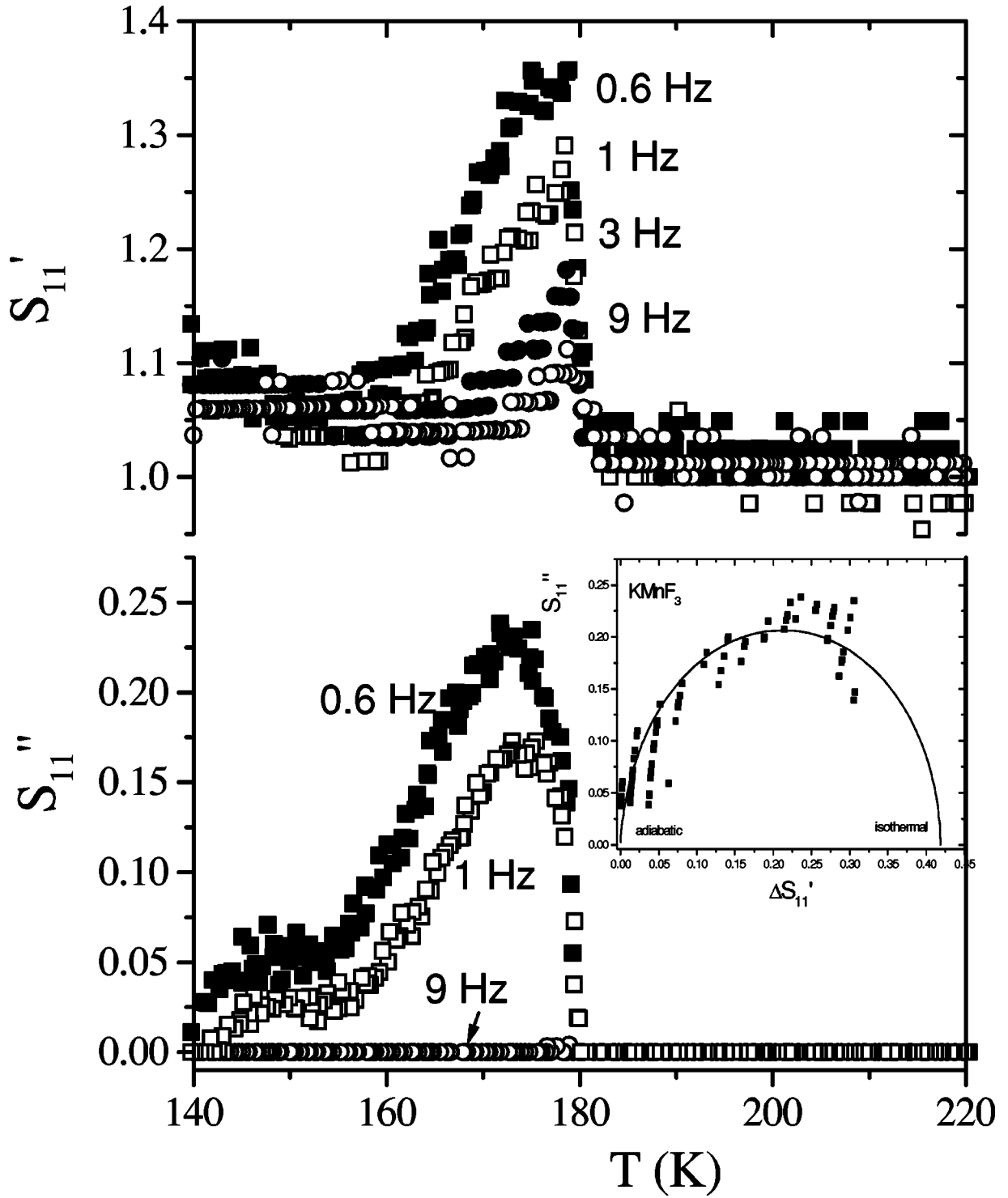


FIG. 3. Temperature dependencies of the real part $S'_{11}(\omega)$ and the imaginary part $S''_{11}(\omega)$ of the complex elastic compliance of pure KMnF_3 in the phase-transition region at various frequencies. The inset shows the temperature-parametrized CC plot.

B. Three point bending mode

where

Here $\hat{\sigma}_3(\mathbf{x}) = \times(2|x_1| - 1) \times \text{const} \times x_3$, and so

$$\frac{(\hat{\sigma}_{3,n}^0)^2}{\|\hat{\sigma}_3\|_{L_2}^2} = \hat{X}_{n_1}^2 \hat{Y}_{n_2}^2 \hat{Z}_{n_3}^2, \quad (69)$$

$$\hat{X}_{n_1} := \frac{\int_{-1/2}^{1/2} dx_1 (2|x_1| - 1) f_{n_1}(x_1)}{\sqrt{\int_{-1/2}^{1/2} dx_1 (2|x_1| - 1)^2}}, \quad (70a)$$

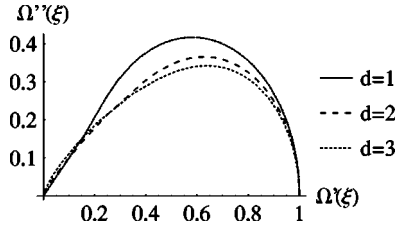


FIG. 4. Comparison of CC plots obtained from $\Omega_{\text{Fally}}^{(d)}(\xi)$ for isothermal boundary conditions in dimensions $d=1-3$.

$$\hat{Y}_{n_2} := \int_{-1/2}^{1/2} dx_2 f_{n_2}(x_2), \quad (70b)$$

$$\hat{Z}_{n_3} := \frac{\int_{-1/2}^{1/2} dx_3 x_3 f_{n_3}(x_3)}{\sqrt{\int_{-1/2}^{1/2} dx_3 x_3^2}}. \quad (70c)$$

From symmetry it follows that Eq. (69) is only nonzero for $n_1=2m_1$, $n_2=2m_2$ even, and $n_3=2m_3-1$ odd. Using the abbreviations $q_1 \equiv q_1(m_1)$, $q_2 \equiv q_2(m_2)$, and $q_3 \equiv q_3(m_3 - 1/2)$, we collect (see Fig. 5)

$$\hat{X}_{2m_1} = 8\sqrt{3}N_o(q_1) \frac{\sin^2\left(\frac{q_1}{4}\right)}{q_1^2}, \quad (71a)$$

$$\hat{Z}_{2m_3-1} = 2\sqrt{3}N_o(q_3) \frac{q_3 \cos\left(\frac{q_3}{2}\right) - 2 \sin\left(\frac{q_3}{2}\right)}{q_3^2}, \quad (71b)$$

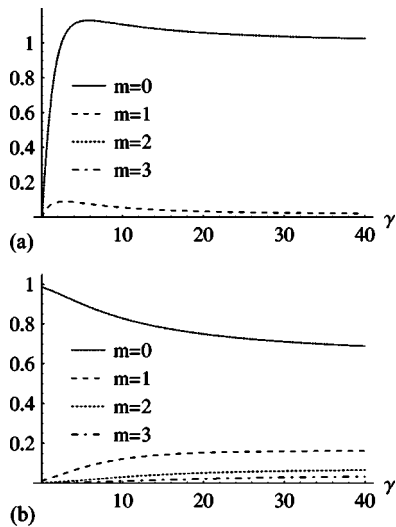


FIG. 5. (a) Coefficients \hat{X}_{2m-1}^2 as functions of γ for $m=1-4$ as determined from Eq. (71a). (b) \hat{Z}_{2m-1}^2 as a function of γ for $m=0-3$ as determined from Eq. (71b).

$$\hat{Y}_{2m_2} = \bar{f}_{2m_2} = 2N_e(q_2) \frac{\sin\left(\frac{q_2}{2}\right)}{q_2}. \quad (71c)$$

In the physically relevant limit of small γ_i one again verifies numerically that the lowest-order contribution $\mathbf{n}=(0,0,1/2)$ dominates the sum (55) by far, and thus we conclude that again $\Omega(\omega)$ should be of the Debye type

$$\Omega(\omega) \sim \frac{1}{1 + i\omega\tau_{(0,0,1/2)}}, \quad (72a)$$

$$\tau_{(0,0,1/2)} = \frac{1}{2Dh} \frac{1}{1/l_1 + 1/l_2 + 2\left(l_3 + \frac{\pi^2}{4h}\right) / l_3^2}. \quad (72b)$$

For $l_3 \ll l_1, l_2$ we obtain

$$\tau_{(0,0,1/2)} \approx \frac{l_3^2}{4Dh\left(l_3 + \frac{\pi^2}{4h}\right)} \approx \frac{l_3^2}{4Dh\left(\frac{\pi^2}{4h}\right)} = \frac{l_3^2}{D\pi^2}. \quad (73)$$

In contrast to the PPM situation, we observe that for 3PB and a platelike specimen of thickness l_3 the lowest (and usually only observable) heat-diffusion relaxation time $\tau_{(1/2,0,0)}$ is independent of h and proportional to l_3^2 . Physically, this illustrates the fact that in 3PB one primarily measures the heat exchange among different regions inside the crystal caused by the presence of inhomogeneous stress, while in the PPM one only observes the heat loss through the crystal's surface.

Again, the above assertions are fully supported by experiment. Consider the example of KSCN crystals,⁸ which undergo an order-disorder phase transition around $T_c=415$ K. Measurements of the complex elastic compliance S_{33} as a function of temperature and frequency yield an ultralow-frequency elastic relaxation below T_c . As shown in Fig. 6, not only is the measured dispersion of a Debye type, but moreover the corresponding characteristic relaxation time, being of an order of 0.1 s of magnitude, is indeed observed to be proportional to l_3^2 , as predicted by Eq. (73).

C. The model of Chaves *et al.*

We now analyze the treatment of heat diffusion given in Ref. 4. Actually, the theory presented there refers to the study of the dielectric susceptibility. Nevertheless, as was mentioned above the theoretical concepts can be taken over to the elastic case in a one-to-one manner.

To circumvent the problem of defining and controlling boundary conditions, in Ref. 4 a crystal of size $|r_i| \leq l_i/2$ subject to a homogeneous TDF is assumed to be surrounded by an infinite medium of the same heat conductivity and heat capacity. Within our present treatment, this actually resembles a crystal of infinite size subject to an inhomogeneous external excitation

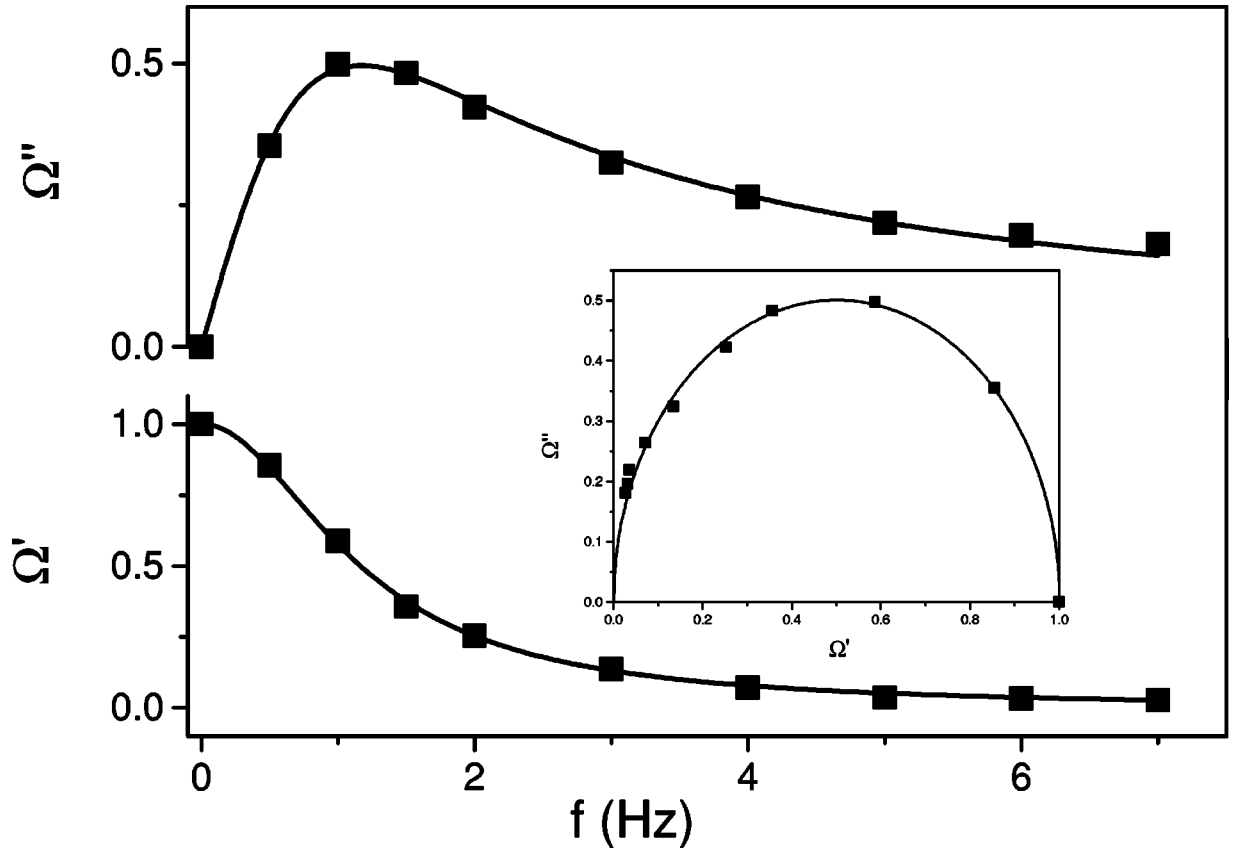


FIG. 6. Frequency dependence of the crossover function $\Omega(\omega)$ of KSCN at $T_c - T = 2$ K as determined from the experimental data of Ref. 8. The lines represent a fit with a Debye dispersion, while the corresponding CC plot is shown in the inset.

$$F(t, \mathbf{r}) = \begin{cases} F(t) & |r_i| \leq l_i/2, \\ 0 & |r_i| > l_i/2. \end{cases} \quad (74)$$

Working out this problem for general TDF $F(t, \mathbf{r})$, we investigate the corresponding heat diffusion equation. In reduced coordinates we consider

$$\frac{\partial u(t, \mathbf{x})}{\partial t} + Lu(t, \mathbf{x}) = \hat{F}(t, \mathbf{x}) \quad (75)$$

with the initial condition $u(0, \mathbf{x}) = 0$. Since no boundary conditions are imposed, there is no restriction on the admissible \mathbf{q} vectors. The solution of Eq. (75) therefore takes the form¹⁴

$$u(t, \mathbf{x}) = \int \frac{d^3 q}{(2\pi)^3} e^{-\lambda_q t} \left[\int_0^t ds \hat{F}_q(s) e^{\lambda_q s} \right] e^{-i\mathbf{q} \cdot \mathbf{x}}, \quad (76)$$

where again $\tau_q^{-1} = \lambda_q := \sum_{i=1}^3 D_i q_i^2$ and

$$\hat{F}_q(s) := \int d^3 x F(s, \mathbf{x}) e^{i\mathbf{q} \cdot \mathbf{x}}. \quad (77)$$

We now specialize our treatment to excitations of type

$$\hat{F}(t, \mathbf{x}) \equiv -\frac{\omega \bar{T} \alpha}{C_\sigma} \hat{\sigma}^0(\mathbf{x}) \sin(\omega t). \quad (78)$$

Then in an obvious notation of

$$\hat{F}_q(s) = -\frac{\omega \bar{T} \alpha}{C_\sigma} \sin(\omega s) \hat{\sigma}_q^0. \quad (79)$$

Since there are no boundary conditions to obey, a review of the corresponding derivation shows that Eq. (22) now holds for $V = \mathbb{R}^3$. Therefore, almost literally repeating the steps of the calculation of Sec. IV C with sums replaced by integrals, we obtain the general crossover function in $d=3$ dimensions,

$$\Omega(\omega) = \frac{1}{\|\hat{\sigma}_0\|_{L_2(\mathbb{R}^3, \mathbb{R})}^2} \int \frac{d^3 q}{(2\pi)^3} \frac{|\hat{\sigma}_q^0|^2}{1 + i\omega \tau_q}. \quad (80)$$

How is this approach related to the one presented above? In Ref. 4 the crossover function of a simple one-dimensional model defined by the steplike spatial excitation function

$$\hat{\sigma}^0(x) := \begin{cases} 1 & |x| < 1/2, \\ 0 & |x| \geq 1/2 \end{cases} \quad (81)$$

was calculated from the response to a steplike excitation in time. Using the present methods, since

$$\|\hat{\sigma}^0\|_{L_2(\mathbb{R}, \mathbb{R})}^2 = 1, \quad \hat{\sigma}_q^0 = \frac{2 \sin(q/2)}{q}, \quad (82)$$

reducing our formula (80) to $d=1$ yields immediately

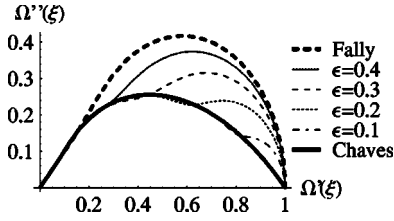


FIG. 7. Comparison of CC plots of $\Omega_\epsilon(\xi)$ for $\epsilon = 1, 0.4, 0.3, 0.2, 0.1, 0.07$, and 0 .

$$\begin{aligned} \Omega_{\text{Chaves}}^{(d=1)}(\xi) &:= \int \frac{dq}{2\pi} \frac{4 \sin^2(q/2)}{q^2} \frac{1}{1 + i\omega/(D_1 q^2)} \\ &= \frac{1 - e^{-(1+i)\sqrt{\xi}}}{(1+i)\sqrt{\xi}}, \end{aligned} \quad (83)$$

where ξ was defined in Eq. (67).

On the other hand, consider a ($d=1$) finite-volume model defined by the excitation function

$$\sigma_{r_0}(t, r) := \begin{cases} \cos(\omega t) & |r| < r_0/2, \\ 0 & |r| \geq r_0/2 \end{cases} \quad (84)$$

with boundary conditions defined by a given heat transfer coefficient h . In reduced units, the spatial part is

$$\hat{\sigma}_\epsilon^0(x) = \begin{cases} 1 & |x| < \epsilon/2, \\ 0 & |x| \geq \epsilon/2, \end{cases} \quad \epsilon := r_0/l_1. \quad (85)$$

Now let us consider the case $l_1 \rightarrow \infty$ for $D_1 = D/l_1^2 = \text{held constant}$. If we simultaneously let $r_0 \rightarrow \infty$ such that $\epsilon = 1$ remains constant, this approaches a system with isothermal ($\gamma_1 = \infty$) boundary conditions, and the corresponding crossover function reduces to $\Omega_{\text{Fally}}^{(d=1)}(\omega)$ as defined by Eq. (67). More generally, if ϵ is kept fixed at a value $\epsilon < 1$, since $\|\hat{\sigma}^0\|_{L_2}^2 = \epsilon$, we obtain the sum

$$\Omega_\epsilon(\omega) := \frac{4}{\pi^2 \epsilon} \sum_{m=0}^{\infty} \frac{1 - \cos[(2m+1)\pi\epsilon]}{(2m+1)^2} \frac{1}{1 + i\omega\tau_{2m}}. \quad (86)$$

A numerical comparison of CC plots shows (cf. Fig. 7) that for $0 \leq \epsilon \leq 1$ the function $\Omega_\epsilon(\xi)$ interpolates between $\Omega_{\text{Chaves}}^{(d=1)}(\xi)$ and $\Omega_{\text{Fally}}^{(d=1)}(\xi)$.

We therefore conclude that the ($d=1$) model of Ref. 4 is equivalent to a one-dimensional crystal of finite volume subject to a deltalike excitation at its center with isothermal boundary conditions. In our opinion, its practical physical relevance for interpreting experimental measurements on single domain crystals is therefore doubtful. Nevertheless, it is of considerable relevance in the study of heat diffusion in random domain distributions, as we shall show below.

D. Considerations for dimensions $d=2,3$

Following a similar approach as that taken in Ref. 4, in Ref. 5 the above model is generalized to one representing a spherically shaped crystalline ‘‘bubble’’ of, say, radius R sur-

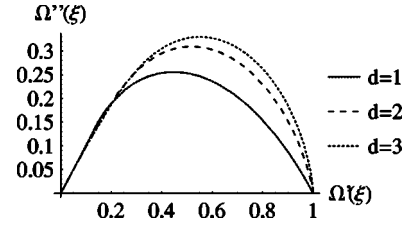


FIG. 8. Comparison of CC plots of $\Omega_{\text{Chaves}}^{(d)}(\xi)$ in dimensions $d=1-3$. The CC plot is of course invariant with respect to the choice $R=1$ of the cluster radius.

rounded by an infinite medium of the same heat capacity and conductivity. The resulting crossover functions can be readily obtained from evaluating the formulas corresponding to Eq. (80) for $d=2$ and $d=3$ in polar coordinates for $D_i = D$, $i=1, \dots, d$. Integrating Eq. (80) for

$$\hat{\sigma}_q^0 = \begin{cases} \frac{2\pi R}{q} J_1(Rq), & d=2, \\ \frac{4\pi}{q^3} [\sin(Rq) - Rq \cos(Rq)], & d=3 \end{cases} \quad (87)$$

and defining another dimensionless angular frequency

$$\xi_R := \frac{R^2 \omega}{2D} \quad (88)$$

we instantly obtain

$$\Omega_{\text{Chaves}}^{(d=2)}(\xi_R) = 2R^2 I_1((1+i)\sqrt{\xi_R}) K_1((1+i)\sqrt{\xi_R}) \quad (89)$$

for $d=2$. Here $J_n(z)$ denotes the Bessel function of the first kind and $I_n(z)$ and $K_n(z)$ denote the modified Bessel functions of the first and second kinds, respectively. For $d=3$, one has

$$\begin{aligned} \Omega_{\text{Chaves}}^{(d=3)}(\xi_R) &= \frac{3}{8} \xi_R^{-3/2} \{1 + i + 2(1-i)\xi_R - [1 + i + 4i\sqrt{\xi_R} \\ &\quad - 2(1-i)\xi_R] e^{-2(1+i)\sqrt{\xi_R}}\}. \end{aligned} \quad (90)$$

Figure 8 shows a CC plot comparison of the crossover functions $\Omega_{\text{Chaves}}^{(d)}$ for $d=1,2,3$.

In closing this section we note the interesting similarity between the CC plots of $\Omega_{\text{Fally}}^{(d=3)}(\xi)$ and $\Omega_{\text{Chaves}}^{(d=3)}(\xi)$ as shown in Fig. 9: While their CC plots are quite distinct in a $d=1$ setting, in $d=3$ a CC plot resulting from the boundary conditions used by Chaves *et al.* is hard to distinguish from that

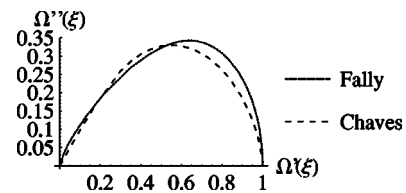


FIG. 9. Comparison of CC plots of $\Omega_{\text{Chaves}}^{(d=3)}(\xi)$ as compared to $\Omega_{\text{Fally}}^{(d=3)}(\xi)$ for $d=3$.

derived from completely isothermal ones for single domain crystals of close to cubic shape.

VI. HEAT DIFFUSION IN POLYDOMAIN CRYSTALS AND DISORDERED SYSTEMS

Up to now we have studied heat diffusion dynamics in the rather restrictive case of a monodomain crystal. However, usually a structural phase transition may be accompanied by the formation of domains and other microstructures. In particular, it is well known that the presence of domain walls often leads to large deviations of the dynamic elastic^{15,16} or dielectric¹⁷ susceptibilities from the monodomain behavior. This may be due to a variety of effects such as e.g., domain-wall motion hindered by various pinning mechanisms^{18–20} and domain freezing.²¹ On the other hand, in the presence of domains heat diffusion inevitably occurs, not only between the crystal and its surrounding but also within different domains, since an external excitation leads to different internal temperature levels. Therefore it comes as no surprise that in real experiments it is often very difficult or impossible to decouple all these different central peak mechanisms. However, note that quite generally the influence of domain-wall motion to macroscopic susceptibilities is proportional to the number of domain walls.^{15,22} Therefore by controlling the domain density by application of an electric or elastic bias field it should be possible to separate heat-diffusion from domain-wall dynamics. In fact, in Ref. 5 non-Debye low-frequency dielectric dispersions were measured in a number of ferroelectric crystals and were attributed to the switching of small polarization clusters or domains. In the following we briefly investigate the problem of heat diffusion dynamics in polydomain crystals.

A. Analytical arguments

To begin, consider the most elementary case of a central domain wall perpendicular to the x_1 direction dividing the crystal into two domains of opposite polarization (\pm). Assume further a TDF $\hat{F}(t, x)$ homogeneous in space. Then, since the actions of $\hat{F}(t, x)$ on both domains will always bear an opposite sign, symmetry demands that the temperature fluctuations must vanish all along the central plane $x_1 = 0$, i.e., $u[t, (0, x_2, x_3)] \equiv 0$. Thus, the physics of heat diffusion in such a crystal should be equivalent to that of heat diffusion in a single domain crystal of just half the original size where *isothermal* boundary conditions are used on one of the surface planes perpendicular to the x_1 direction. The situation is reminiscent of the method of mirror charges used in electrostatic boundary problems.

In $d = 1$ it is instructive to investigate this analytically for the simple case of isothermal boundary conditions. We introduce the inhomogeneous function

$$\hat{F}^0(x) = \frac{\hat{\sigma}^0 \alpha \bar{T}}{C_\sigma} \times \begin{cases} +1 & -1/2 < x < 0, \\ -1 & 0 \leq x < 1/2 \end{cases} \quad (91)$$

in reduced coordinates. Since this is odd with respect to x , the corresponding projection coefficients $\hat{F}_{q(n)}^0$ will only be

nonzero for odd $n = 2m - 1$. Using $\tau_{2m-1}^{-1} = D_1(2m\pi)^2$ and calculating the projection coefficients

$$\hat{F}_{q(2m-1)} = \hat{\sigma}^0 \frac{\alpha \bar{T}}{C_\sigma} \frac{\sqrt{2}}{m\pi} [(-1)^m - 1] \quad (92)$$

we therefore obtain the dispersion

$$\Omega(\omega; 2) := \sum_{m=1}^{\infty} \frac{\frac{2}{m^2 \pi^2} [(-1)^m - 1]^2}{1 + \frac{i\omega}{4D_1 m^2 \pi^2}} = \Omega_{\text{Fally}}(\xi(2)), \quad (93)$$

where we define

$$\xi(2) := \frac{\omega}{8D_1} = \frac{\omega}{2(4D_1)}. \quad (94)$$

In effect, compared to formula (67), $D_1 = D/l_1^2$ is replaced by $4D_1 = 4D/l_1^2 = D/(l_1/2)^2$, such that actually l_1 is replaced by $l_1/2$.

On the other hand, consider our former model monodomain crystal subject to a spatially homogeneous excitation. Since the boundary conditions are symmetric with respect to $x_1 \rightarrow -x_1$, the heat flow through the central plane $x_1 = 0$ must be zero, i.e.,

$$q(0, x_2, x_3) = -\kappa(0, \partial_u / \partial x_2, \partial_u / \partial x_3). \quad (95)$$

The heat diffusion dispersion of such a crystal is therefore obviously equivalent to that of a homogeneous crystal with the replacement $l_1 \rightarrow l_1/2$ and *adiabatic* boundary conditions imposed perpendicular to the x_1 direction on one of the two surfaces, while h is kept fixed on the other.

These observations are quite useful for a qualitative and quantitative study of heat diffusion in more general domain distributions. However, a thorough investigation of the problem involving, e.g., different domain orientations is beyond the scope of the present paper. In the following we confine ourselves to the two extreme cases of a *regular periodic* pattern of domains of alternating polarization as compared to systems with a *random statistical* distribution of such domains.

1. Regular domain pattern

Let $M \in \mathbb{N}$. We define the following symmetric partition of the interval $I := [-1/2, 1/2]$, which describes $2M - 1$ one-dimensional domains of polarization $\propto (-1)^{M+\nu}$ and size $1/(2M)$ enclosed by two domains of polarization $\propto (-1)^M$ and size $1/(4M)$ at the boundary (cf. Fig. 10):

$$I = \left[-\frac{1}{2}, -\frac{1}{2} + \frac{1}{4M} \right) \cup \left[-\frac{1}{2} + \frac{4M-1}{4M}, \frac{1}{2} \right] \cup \left\{ \bigcup_{\nu=1}^{2M-1} \left[-\frac{1}{2} + \frac{2\nu-1}{4M}, -\frac{1}{2} + \frac{2\nu+1}{4M} \right] \right\}. \quad (96)$$

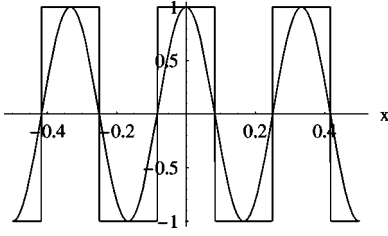


FIG. 10. Periodic domain distribution according to Eq. (96) for $M=3$ vs $f_6(x)$.

Let $\theta_{[a,b]}(x)$ denote the characteristic function of the interval $[a,b]$. Then a homogeneous external excitation $\hat{\sigma}(t,x) = \hat{\sigma}^0(x)\cos(\omega t)$ yields an effective TDF $\hat{F}(t,x)$ with a spatial part

$$\begin{aligned} \hat{F}^0(x) = & \frac{\hat{\sigma}^0 \alpha \bar{T}}{C_\sigma} \left\{ (-1)^M \theta_{[-(1/2), -(1/2)+(1/4M)]}(x) \right. \\ & + \sum_{\nu=1}^{2M-1} (-1)^{M+\nu} \\ & \times \theta_{[-(1/2)+(2\nu-1/4M), -(1/2)+(2\nu+1/4M)]}(x) \\ & \left. + (-1)^M \theta_{[-(1/2)+(4M-1/4M), (1/2)]}(x) \right\} \quad (97) \end{aligned}$$

in reduced coordinates. Note that trivially $\|\hat{\sigma}\|_{L_2}^2 = (\hat{\sigma}^0 \alpha \bar{T}/C_\sigma)^2$. Due to inversion symmetry only the even base functions $f_{2m}(x)$ are relevant. According to the above observations, in the limit of adiabatic boundary conditions where the heat flow on the boundary is assumed to be zero, the two “small” boundary domains can be merged to one single domain. Moreover, symmetry and orthogonality of the base functions $f_n(x)$ demands that the temperature fluctuations $u(t,x)$ must vanish along all the domain walls $x_1 \equiv -\frac{1}{2} + (2\nu-1)/4M$. Symmetry also singles out the base functions $f_{2m}(x) = \sqrt{2} \cos[2m\pi x]$ for adiabatic boundary conditions, and, projecting the resulting pattern of $N:=2M$ domains onto these base functions, one obtains the coefficients

$$\hat{\sigma}_{q(2m)}^0 = \frac{\alpha \bar{T}}{C_\sigma} \begin{cases} (-1)^{i+1} \frac{2\sqrt{2}}{(2i-1)\pi} & m=(2i-1)M, \\ 0 & \text{else.} \end{cases} \quad (98)$$

From this one explicitly computes

$$\Omega(\omega; N) := \frac{1}{\|\hat{\sigma}^0\|_{L_2}^2} \sum_{m=0}^{\infty} \frac{[\hat{\sigma}_{q(2m)}^0]^2}{1+i\omega\tau_{2m}} = \Omega_{\text{Fally}}(\xi(N)), \quad (99)$$

where we generalize

$$\xi(N) := \frac{1}{N^2} \frac{\omega}{2D_1}. \quad (100)$$

The corresponding characteristic relaxation time is

$$\tau(N) \approx \frac{1}{5} \frac{(l_1/N)^2}{2D} = \frac{\tau_{\text{Fally}}}{N^2}. \quad (101)$$

We thus conclude that the system can effectively be regarded as a homogeneous one with *isothermal* boundary conditions which has been shrunk from length l_1 to l_1/N .

2. Random domain pattern

Suppose now that the crystal displays a domain pattern of complete random nature. Next, we pick a single one of these domains not too close to the crystal's boundary and call it domain \mathcal{D}_μ . In contrast to the strictly regular scenario, the presence the neighboring domains then does not yield strict boundary conditions for the isolated system \mathcal{D}_μ such as in the regular case where the temperature deviation $u(x)$ is forced to be zero. However, suppose first that \mathcal{D}_μ is rather small as compared to its surrounding neighbors $\mathcal{D}_{\mu-1}, \mathcal{D}_{\mu+1}$. Then, recalling the interpretation at the end of Sec. V C, we realize that in good approximation domain \mathcal{D}_μ represents a system of just the type investigated there (but with a doubled temperature difference of the system and surrounding). On the other hand, if \mathcal{D}_μ is surrounded by a number of smaller domains $\mathcal{D}_{\mu-i}, \dots, \mathcal{D}_{\mu+i}$, domain \mathcal{D}_μ can also be thought of as residing in a thermal environment of average temperature \bar{T} , i.e., $u(x)=0$ and thermal conductivity and diffusivity identical to that of itself, since the external excitation induces polarization-dependent temperature deviations in the surrounding domains $\mathcal{D}_{\mu-i}$ which quickly cancel on the average by “destructive thermal interference.” These observations lead to the conclusion that while in a real crystal with a given irregular domain pattern the crossover function should be expected to be of a quite distinguished form individually dependent on the very details of this pattern, the “average” crossover function of a large number of such crystals should indeed bear considerable similarity to the crossover function $\Omega_{\text{Chaves}}(\xi)$, where ξ roughly scales with an average domain width.

B. Numerical investigations

Due to its symmetry, the partition underlying Eq. (97) proves to be useful for analytic calculations at adiabatic boundary conditions. For numerical studies of the effect of more general boundary conditions and statistically distributed domain patterns the following partition of I into N sections I_μ of length $1/N$ proves to be more convenient:

$$I = \cup_{\mu=1}^N I_\mu, \quad I_\mu := \left[-\frac{1}{2} + \frac{\mu-1}{N}, -\frac{1}{2} + \frac{\mu}{N} \right]. \quad (102)$$

For a given number $N \in \mathbb{N}$ there exist 2^N possible domain configurations P_ν , $\nu=1, \dots, 2^N$, defined by $P_\nu := (P_{\mu\nu})_{\mu=1}^N$, where $P_{\mu\nu}$ defines the polarization of I_μ in configuration P_ν . Suppose that the system takes on the configuration P_ν . Then effectively the action of the homogeneous TDF $\hat{F}(t,x)$ on the inhomogeneous system is equivalent to that of the inhomogeneous TDF with a spatial part

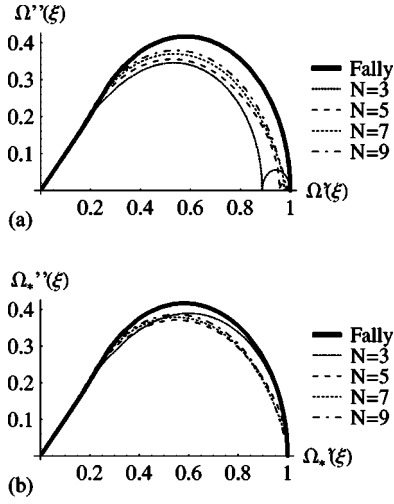


FIG. 11. (a) CC plots of $\Omega(\omega; N)$ computed for the effective TDF defined by Eqs. (103) and (105) for $\gamma=0.001$ and $N=3, 5, 7$, and 9 . (b) Similar for $\Omega_*(\omega; N)$, which is calculated from $\Omega(\omega; N)$ by removing the $q(0)$ -mode contribution and renormalizing the resulting function to 1 at $\omega=0$.

$$\hat{F}(x; P_\nu) := -\frac{\hat{\sigma}_0 \alpha \bar{T} \omega}{C_\sigma} \sum_{\mu=1}^N P_{\mu\nu} \theta_{I_\mu}(x) \quad (103)$$

on a homogeneous system. The configuration P_ν then yields a crossover function

$$\Omega(\omega; P_\nu) := \sum_{n=0}^{\infty} \left[\sum_{\mu=1}^N P_{\mu\nu} \int_{I_\mu} dx f_n(x) \right]^2 \frac{1}{1 + i\omega\tau_n}. \quad (104)$$

We now fix N and consider the following two extremal cases

1. Regular domain pattern

We assume that the system's configuration P_ν is given by N alternately polarized domains in a strictly regular pattern, i.e.,

$$P_{\mu\nu} = (-1)^\mu. \quad (105)$$

Of course in such a system not only the heat exchange between domains [q^α (wave vector of domain pattern)] but also the additional heat loss through the surface due to the mode $q=q(\mathbf{0})$ contributes to $\Omega(\omega)$. For N even Eq. (103) is an odd function of x and vice versa. We conclude that for small and odd N there is a noticeable contribution for $q=q(\mathbf{0})$. Indeed, numerical computations of CC plots of the resulting dispersion, which we write as $\Omega(\omega; N)$, for various values of N odd reveal an additional small half circle for N odd in the physically interesting case $\gamma_i \ll 1$, as illustrated by Fig. 11.

For growing values of N , the CC plots of $\Omega(\omega; N)$ rapidly approach that of $\Omega_{\text{Fally}}(\omega)$, which comes as no surprise as we argued above. On the other hand, for N not too large an additional low-frequency Debye-like contribution $\propto [\hat{F}_{q(\mathbf{0})}^0(N)]^2 / (1 + i\omega\tau_0)$ is visible since the projection coefficient $\hat{F}_{q(\mathbf{0})}^0(N) \approx \hat{F}^0(N)$ cannot be neglected for small and odd N . However, the accompanying relaxation time τ_0

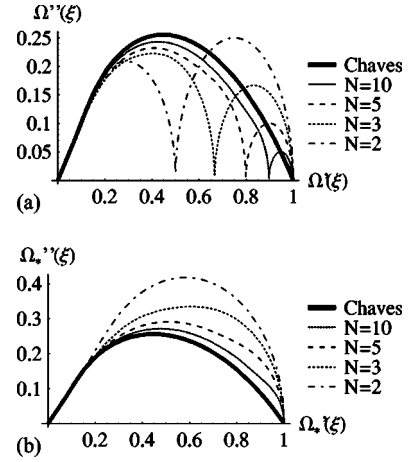


FIG. 12. (a) CC plots of $\langle \Omega \rangle_N(\xi)$ for $\gamma=0.001$ and $N=2, 3, 5$, and 10 compared to that of $\Omega_{\text{Chaves}}(\xi)$. (b) Similar for $\Omega_*(\omega)$, which is calculated from $\Omega(\omega)$ by removing the $q(0)$ -mode contribution and renormalizing the resulting function to 1 at $\omega=0$.

$\approx (2 \sum_i D_i \gamma_i)^{-1} = (2Dh \sum_i 1/l_i)^{-1}$ [cf. Eq. (35a)] is usually large and therefore frequently remains undetected in experiment.

2. Random domain pattern

Suppose that the domain pattern is completely random and we consider the averaged crossover function

$$\langle \Omega \rangle_N(\omega) := \frac{1}{2^N} \sum_{\nu=1}^{2^N} \Omega(\omega; P_\nu) \quad (106)$$

over all possible configurations P_ν with polarizations $P_{\mu\nu} = \pm 1$, $\mu=1, \dots, N$. In this case N should of course not be confused with the number of domains, but rather it labels the coarseness of our hypothetical grid of domains. In fact, it is not hard to see that for such model systems the average domain size in reduced units is

$$\frac{2(1-2^{-N})}{N} \sim \frac{2}{N} \text{ for } N \gg 5. \quad (107)$$

We thus conclude that for large N this averaging model should yield a crossover function $\langle \Omega \rangle_N(\xi)$, whose CC plot approaches that of $\Omega_{\text{Chaves}}(\xi)$ and a typical maximum value ξ_{max} of $\langle \Omega \rangle_N''(\xi)$ proportional to N^2 with increasing accuracy for growing N . For numerical tests of these assertions see Figs. 12 and 13.

In Ref. 5 the measured low frequency dielectric permittivity of Rochelle salt, triglycine sulfate, BaTiO_3 , and potassium dihydrogen phosphate near their phase-transition temperatures was attributed to heat diffusion and fitted to the crossover function $\Omega_{\text{Chaves}}(\xi)$. However, the authors note that this behavior cannot be interpreted as a monodomain response and conflicts with the boundary conditions represented by the measuring setup. While no explicit calculations are made, they speculate on the role of heat exchange between microdomains. Indeed, as we theoretically showed

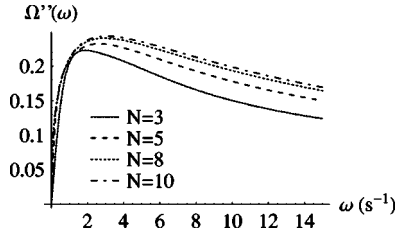


FIG. 13. Comparison of the negative imaginary part of the random domain crossover function $\langle \Omega \rangle_N(N^2\xi)$ for $N=3, 5, 8,$ and 10 .

above, the appearance of $\Omega_{\text{Chaves}}(\xi)$ is not at all in conflict with the experimental boundary conditions but can also neatly be understood as heat diffusion in irregular domain patterns. On the other hand, the enhancement of the measured central peak intensity is also consistent with a multi-domain response as a result of additional domain wall motion.

C. Heat diffusion for spherically shaped clusters

In closing this section, let us review the interesting results of Ref. 5 in the context of the theory presented above. In Ref. 5, a “raisins in a cake” model of well-separated spherically shaped isotropic clusters, which are susceptible to an external excitation (i.e., $\alpha_i = \alpha \neq 0, i=1-3$ inside the bubbles), surrounded by an infinite medium of identical heat capacity and conductivity, is studied. The corresponding crossover function was calculated as Eq. (90) of Sec. V D. After a simple transformation of variables $\tau = (Dq^2)^{-1}$ in Eq. (80) we read off the spectral representation

$$\Omega_{\text{Chaves}}^{(d=3)}(\omega) = \int_0^\infty \frac{d\tau}{\tau} \frac{g(D\tau/R^2)}{1+i\omega\tau}, \quad (108)$$

where

$$g(\theta) = \frac{3}{\pi} \sqrt{\theta} (\cos \sqrt{1/\theta} - \sqrt{\theta} \sin \sqrt{1/\theta})^2. \quad (109)$$

As illustrated by Fig. 14, the widespread distribution of $g(\theta)$, which displays an infinite series of rapidly descending maxima, illustrates the non-Debye character of the dispersion function (108). The lowest dimensionless frequency $\theta^{-1} \approx 6.0569$ corresponding to the largest maximum of $g(\theta)$

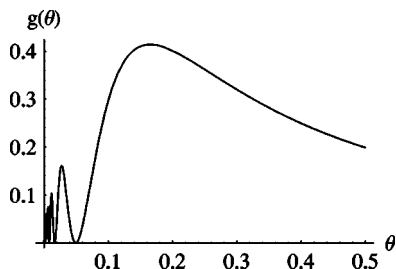


FIG. 14. Plot of the spectral function $g(\theta)$ as defined by Eqs. (108) and (109).

at $\theta \approx 0.1651$ is necessarily somewhat higher than the absorption maximum value $\xi_R \approx 5.0542$ of the negative imaginary part of $\Omega_{\text{Chaves}}^{(d=3)}(\omega)$.

In Ref. 5 the above approach is proposed to describe heat diffusion among “clusters” of various physical origins. In particular, an overall response function is introduced by averaging the single cluster dispersion (108) over a probability distribution $n(R)$ of clusters of radii R as obtained from, e.g., percolation theory. The resulting dispersion is claimed to be rather insensitive to the choice of such $n(R)$ and fitted to the Laplace transform of a stretched exponential-type relaxation $\sim e^{-(t/\tau_0)^\beta}$ with $\beta \sim 0.6$.

Obviously, the above approach can be applied to study, e.g., heat diffusion caused by ferroelectric domains in cases where the domain structure is effectively spherical rather than that of one-dimensional layers. However, the results have to be taken with a grain of salt. On the one hand, in calculating the response of a multisphere system by averaging the single cluster response over a partition $n(R)$ of radii R , the authors knowingly neglected the mutual thermal interaction of these spheres, while in Sec. VI A 1 we recognized the “mirror effect” appearing in regular patterns of (\pm) domains to be important in such systems. Additional concerns regarding the applicability of such an approach to structures of mesoscopic dimensions were also noted. Nevertheless, we conjecture that the above approach could be quite useful to study, e.g., heat diffusion between precursor clusters near phase transitions, whose radius is governed by a strongly T -dependent correlation length $\xi(T)$, and where disturbances stemming from domain-wall dynamics/freezing are absent in the symmetrical phase. In this context, we would like to draw attention to the results of Ref. 23 on low-frequency elastic measurements in C_{60} single crystals, where a crossover from isothermal-to-adiabatic elastic constants was indeed observed as a precursor to the phase transition and attributed to heat diffusion. To completely clarify this conjecture in the present theoretical context, work is in progress.

VII. DISCUSSION

The preceding sections have shown how multifaceted is the appearance of heat diffusion in single domain crystals at various types of boundary conditions and polydomain crystals or heterogeneous systems. For PPM and 3PB experiments on macroscopic monodomain crystals we have demonstrated that for physically acceptable boundary conditions the observed relaxation will necessarily be of a Debye type with a characteristic dependence on the sample’s geometry [cf. Eqs. (66) and (72)]. For dielectric experiments, one cannot completely rule out the possibility of isothermal boundary conditions, in which case the crossover function (67) would be found. All other experimental appearances of non-Debye-like relaxations for macroscopic monodomain crystals must necessarily be either attributed to heat diffusion within polydomain structures and/or other processes of other physical origin such as order-parameter dynamics, domain-wall motion, or domain freezing. Other dispersions may appear for cases of extremely anisotropic geometry such as

e.g., in thin crystalline films. As far as pure heat diffusion in crystals with layered polydomain structures is concerned, the crossover functions (67) and (83) describe two extremal situations of either a strictly regular domain sequence or an average over a large number of samples with random domain patterns. Heat diffusion originating from spherical clusters is yet another story.

Despite its universal presence, in experiment the effects of heat diffusion are frequently contaminated by large contributions resulting from domain-wall motion, domain freezing, or additional order-parameter dynamics, and usually neither the distinction of Debye vs non-Debye relaxation, nor a particular shape of the CC plot or the low frequency nature of a measured effect can alone be regarded as clear evidence. However, although we have determined a diversity of quite different dispersion functions all originating from heat diffu-

sion, their accompanying frequency behavior always shows a distinct *size and geometry dependence* reflecting

- the macroscopic dimensions of the sample,
- the typical length scale of domains or clusters under investigation or,
- the experimental wavelength with which the sample is probed.

In fact, experimental observation⁸ of this characteristic dependence serves as decisive evidence to distinguish heat diffusion from other effects.

ACKNOWLEDGMENTS

Support from Österreichischer Fonds zur Förderung der Wissenschaftlichen Forschung (Project No. P15016-PHY) is gratefully acknowledged.

*Electronic address: troester@ap.univie.ac.at

¹M.D. Mermelstein and H.Z. Cummins, Phys. Rev. B **16**, 2177 (1977).

²K.B. Lyons and P.A. Fleury, Phys. Rev. Lett. **37**, 161 (1976).

³E. Riste, J. Samuelsen, K. Otnes, and J. Feder, Solid State Commun. **9**, 1455 (1971).

⁴A.S. Chaves, F.V. Letelier, J.F. Sampaio, and R. Gazinelli, Phys. Rev. B **47**, 4880 (1993).

⁵J.F. Araujo, J. Mendes Filho, F.E.A. Melo, F.V. Letelier, and A.S. Chaves, Phys. Rev. B **57**, 783 (1998).

⁶A.S. Chaves, J.F. Sampaio, V.B. Kokshenev, and M.C. Nemes, J. Phys. Soc. Jpn. **66**, 1015 (1997).

⁷M. Fally, W. Schranz, and D. Havlik, Phys. Rev. B **53**, 14 769 (1996).

⁸W. Schranz and D. Havlik, Phys. Rev. Lett. **73**, 2575 (1994).

⁹W. Schranz, A. Tröster, A. V. Kityk, P. Sondergeld, and E. K. H. Salje (unpublished).

¹⁰L.D. Landau and E.M. Lifschitz, *Lehrbuch der Theoretischen Physik* (Akademie-Verlag, Berlin, 1989) Vol. VII, p. 100.

¹¹R. Courant and D. Hilbert, *Methoden der Mathematischen Physik II* (Springer, Berlin, 1968).

¹²W. I. Smirnow, *Lehrgang der Höheren Mathematik* (Deutscher Verlag, Berlin, 1979), Vol. IV.

¹³J. F. Santarius *et al.*, University of Wisconsin Fusion Technology

Institute Report No. UWFD-1129, 2000 (unpublished).

¹⁴From this, one easily derives the well-known convolution representation $u(t, \mathbf{x}) = \int_0^t ds \int d^3y G(t-s, \mathbf{x}-\mathbf{y}) \hat{F}(s, \mathbf{y})$, where

$$G(t-s, \mathbf{x}-\mathbf{y}) := \frac{1}{\pi^{3/2}} \prod_{i=1}^3 \frac{\exp\left[-\frac{(x_i-y_i)^2}{4D_i(t-s)}\right]}{\sqrt{4D_i(t-s)}} \quad (110)$$

is the celebrated *heat kernel*.

¹⁵A.V. Kityk, W. Schranz, P. Sondergeld, D. Havlik, E.K.H. Salje, and J.F. Scott, Phys. Rev. B **61**, 946 (2000).

¹⁶A.V. Kityk, W. Schranz, P. Sondergeld, D. Havlik, E.K.H. Salje, and J.F. Scott, Europhys. Lett. **50**, 41 (2000).

¹⁷Y.N. Huang *et al.*, Phys. Rev. B **55**, 16 159 (1997).

¹⁸T. Nattermann, Y. Shapir, and J. Vilfan, Phys. Rev. B **42**, 8577 (1990).

¹⁹V. Mueller, Y. Shchur, H. Beige, S. Mattauch, J. Glinemann, and G. Heger, Phys. Rev. B **65**, 134102 (2002).

²⁰V. Mueller, Y. Shchur, H. Beige, A. Fuith, and S. Stepanov, Europhys. Lett. **57**, 107 (2002).

²¹M. Fally, P. Kubinec, A. Fuith, H. Warhanek, and C. Filipic, J. Phys.: Condens. Matter **7**, 2195 (1995).

²²A.S. Sidorkin, J. Appl. Phys. **83**, 3762 (1998).

²³P. Dolinar and W. Schranz, Phys. Rev. B **56**, 8566 (1997).